JGR Solid Earth

RESEARCH ARTICLE
10.1029/2023JB027762

Transient Creep of Quartz and Granulite at High Temperature Under Wet Conditions

Sagar Masuti[1], Jun Muto[2], and Erik Rybacki[1]

[1]GFZ German Research Centre for Geosciences, Potsdam, Germany, [2]Tohoku University, Sendai, Japan

Key Points:

- Transient creep flow law parameters of quartz and granulite are determined using a Markov chain Monte Carlo method
- Low stress exponent of the transient creep in silicates could be due to weak dependency of dislocation density on the stress
- Transient creep could be dominant during the postseismic phase of the earthquake cycle

Supporting Information:

Supporting Information may be found in the online version of this article.

Correspondence to:

S. Masuti,
sagar.masuti@gmail.com

Citation:

Masuti, S., Muto, J., & Rybacki, E. (2023). Transient creep of quartz and granulite at high temperature under wet conditions. *Journal of Geophysical Research: Solid Earth*, *128*, e2023JB027762. https://doi.org/10.1029/2023JB027762

Received 31 AUG 2023
Accepted 26 SEP 2023

Author Contributions:

Conceptualization: Sagar Masuti
Data curation: Sagar Masuti, Jun Muto
Formal analysis: Sagar Masuti
Methodology: Sagar Masuti
Software: Sagar Masuti
Supervision: Jun Muto, Erik Rybacki
Writing – original draft: Sagar Masuti
Writing – review & editing: Jun Muto, Erik Rybacki

Abstract Transient creep of crustal rocks is important to explain time-dependent geological processes such as postseismic deformation following a large continental earthquake. While the steady-state creep flow law parameters of quartz and feldspar, major minerals in the upper and lower crust, are well known, the physical mechanism behind transient creep and the corresponding flow law parameters are poorly understood. We quantify the flow law parameters for both quartz and granulite (mixture of plagioclase and pyroxene) under wet conditions with a nonlinear Burgers model using a Markov chain Monte Carlo (MCMC) method. Modeling results yield an activation energy of 70 ± 20 kJ/mol and a stress exponent of 2.0 ± 0.1 for transient creep of quartz aggregates. For granulite/feldspar, we find activation energies of 280 ± 30 and 220 ± 20 kJ/mol and stress exponents of 1.0 ± 0.2 and 0.9 ± 0.1 under mid (1050–1100°C) and high (1125–1150°C), temperature conditions, respectively. The stress exponents and activation energies of transient creep are consistently smaller than those of steady-state creep for both quartz and granulite/feldspar. Combined with results for transient creep of olivine that were previously obtained (Masuti & Barbot, 2021, https://doi.org/10.1186/s40623-021-01543-9), we suggest that the activation energies and stress exponents of transient creep are smaller than those of steady-state creep for volumetrically important silicate minerals of the crust and upper mantle. Extrapolation of the estimated flow law parameters of granulite/feldspar to natural conditions suggests that transient creep may dominate during the postseismic period and lasts longer than previously thought.

Plain Language Summary Earthquakes induce intermittent deformation of the solid Earth at rates that are higher or lower than the interseismic strain rates. When an earthquake occurs, it is accompanied by a sudden slip on the fault and a rapid stress change in the lower crust leading to an evolving rock strength. Lower crustal rocks represent a complex assembly of minerals and several different micro-mechanisms may be activated during deformation. We use experimental data for quartz and feldspar to constrain the mechanical properties of the transient creep (i.e., stress changes with strain under constant strain rate conditions or strain changes nonlinearly with time under constant stress conditions). Based on our results, we conclude that the transient creep following an earthquake may not be as short lived as previously has been thought.

1. Introduction

Postseismic deformation following an earthquake have been examined using linear (e.g., Deng et al., 1998; Diao et al., 2011) or nonlinear steady-state rheologies (e.g., Freed & Bürgmann, 2004). However, transient creep laws are likely to govern the deformation during the postseismic phase of the earthquake cycle (e.g., Agata et al., 2019; Dhar & Muto, 2023; Dhar et al., 2022, 2023; Freed et al., 2010; J. Fukuda & Johnson, 2021; Muto et al., 2019; Masuti et al., 2016; Pollitz, 2003, 2005, 2012; Qiu et al., 2018; Tang et al., 2019). Recent studies have modeled the postseismic geodetic data assuming the same stress and temperature sensitivity for both transient and steady-state creep (e.g., Agata et al., 2019; Masuti et al., 2016; Muto et al., 2019). However, it has been found that the transient and steady-state creep flow law parameters are different in the case of olivine aggregates (Masuti & Barbot, 2021) based on an analysis of laboratory data by using a constitutive framework representing a Burgers model, where the dashpots have the Arrhenius type of relationship for strain rate and is nonlinearly dependent on stress (see also Supporting Information S1). Determining these relationships is important for crustal minerals of the lithosphere, as geodynamic models are developed for a number of problems where stresses and strain rates are not constant.

In order to determine flow law parameters, laboratory experiments are usually conducted on different crustal and mantle minerals such as quartz, feldspar, and olivine. Quartz and feldspar are the most abundant mineral constituents in the upper and lower crust, respectively, and olivine is most abundant in the upper mantle. Unfortunately, most of the experiments performed so far aimed to explore the steady state creep flow parameters, where stress

and strain rate are almost constant after some initial strain. At low strain, however, the rate response is non-linear resulting in transient behavior until steady state conditions are achieved (see Supporting Information S1). What we know of the transient creep largely comes from studies on olivine (e.g., Chopra, 1997; S. Karato, 1998; Hansen et al., 2019; Masuti & Barbot, 2021; S.-I. Karato, 2021). Although several studies have illuminated the transient microstructural development of crustal rocks imposed by sudden stress changes (e.g., C. A. Trepmann et al., 2007; C. Trepmann & Stöckhert, 2013), the detailed mechanical properties of transient creep of quartz and feldspar has not been explored yet. Moreover, transient creep of feldspar is of great importance, the dominant mineral of the lower crust, as studies have shown that viscoelastic relaxation of the lower crust is the dominant mechanism of transient postseismic deformation (e.g., Pollitz et al., 2017).

Laboratory experiments are conducted at different temperatures and strain rates. Typical temperatures at which creep experiments on silicate rocks are conducted vary from 600 to 1200°C and strain rates from 10^{-3} to 10^{-7} s^{-1}. From these experiments, steady-state flow law parameters have been determined using a flow law of the following form (e.g., Hirth & Kohlstedt, 2003; Jung & Karato, 2001)

$$\dot{\varepsilon}_{ss} = A_{ss}\sigma^{n_{ss}} d^{-p_{ss}} \exp\left(-\frac{E_{ss}}{RT}\right), \tag{1}$$

where the subscript ss stands for steady-state, $\dot{\varepsilon}_{ss}$ is the strain rate, A_{ss} is the pre-exponential factor, σ is the differential stress, n_{ss} is the stress exponent, E_{ss} is the activation enthalpy, R is the universal gas constant, T is absolute temperature, and d and p_{ss} are the grain size and its exponent, respectively. In general, the above relationship captures both diffusion (i.e., $n_{ss} = 1$ and $p_{ss} = 2$ or 3) and dislocation creep (i.e., $n_{ss} = 3$ and $p_{ss} = 0$). Laboratory experiments have been conducted on both quartz and feldspar to estimate the stress, grain size, temperature, pressure, and water content (fugacity) dependency (e.g., Chen et al., 2021; Dimanov et al., 1999; Hirth et al., 2001; Luan & Paterson, 1992; Rutter & Brodie, 2004; Rybacki & Dresen, 2000; Rybacki et al., 2006; Tullis et al., 1996; Zhou et al., 2017). The true value of grain size exponent, stress exponent, and activation enthalpy are still being discussed for quartz (see Tokle et al., 2019, for more details). In addition, close to the boundary of diffusion and dislocation creep a combination of these processes or dislocation accommodated grain boundary sliding (disGBS) as an additional deformation mechanism (i.e., $n_{ss} > 1$ and $p_{ss} \approx 2$) has also been observed in quartz (e.g., J.-I. Fukuda et al., 2018; Richter et al., 2018) and in feldspar (e.g., Závada et al., 2007). Recently, a very low stress exponent of ∼0.5 was reported during the development of weak shear zones in feldspar (J. Fukuda et al., 2022). Nevertheless, the steady-state flow law parameters for both quartz and feldspar are considered to be well known and the transient creep flow law parameters are still unknown. Aims of this study are to fit the high-resolution stress versus strain series data of quartz and feldspar with a nonlinear Burgers model, explain the obtained transient creep flow law parameters with a theoretical model, and discuss implication with respect to postseismic deformation.

2. Data

Laboratory experiments are usually conducted under constant load (i.e., stress) or constant displacement rate (i.e., strain rate) conditions. In the case of constant load experiment, the deformation begins with transient behavior, where the strain-rate changes continuously and eventually achieves steady-state, where strain-rate is constant. Determination of steady-state creep is often tricky because the slope of the displacement versus time curve (i.e., apparent strain rate) might appear linear depending on the x- and y-axis, whereas the deformation may be still in transient regime if corrected for the continuous increase in sample diameter assuming constant volume deformation. In the case of a constant imposed strain rate, stress changes until steady-state is reached and stress is constant. Here, we mainly consider constant strain rate data to estimate transient creep flow parameters of quartz and granulite. For quartz, we use data from Gleason and Tullis (1995), where experiments on quartz aggregates were performed in a Griggs apparatus with a molten salt assembly. The molten salt assembly has a better stress resolution that is, ±10 MPa (Holyoke III & Kronenberg, 2010) compared to the traditionally used solid salt assembly. Gleason and Tullis (1995) used Black Hills quartzite with a grain size of about 100 μm. All samples were deformed under wet conditions with an average water content of 0.15 wt.% H_2O. Constant strain rate experiments were conducted at temperatures between 900 and 1100°C and high confining pressures of 1.5–1.7 GPa.

For feldspar, we use data from Zhou et al. (2017), who conducted experiments on granulite at different strain rates and temperatures. Granulite sample composition was mainly plagioclase (∼52%) and pyroxene (∼40%) with

other minor minerals include magnetite and ilmenite (~5%), and quartz (~3%) with a grain size of 100–300 μm. Granulite samples were deformed under wet conditions and the samples had an average water content of 0.17 ± 0.05 wt% H_2O. All the experiments were conducted at constant strain rate starting from a high strain rate of 5×10^{-5} s^{-1} down to a final strain rate of 3.3×10^{-6} s^{-1} in steps of 2.5×10^{-5} s^{-1}, 1.25×10^{-5} s^{-1}, and 6.25×10^{-6} s^{-1} (See Figures 5 and 6). Based on the microstructural observations and mechanical data, (Zhou et al., 2017) found that the granulite aggregate deformed in three different regimes depending on temperature and categorized them as low (900–1000°C), mid (1050–1100°C), and high temperature regimes (1125–1150°C). Flow stresses in each of these regimes were ~600–800 MPa, ~250–450 MPa, and ~80–120 MPa, respectively. At low temperature, they found microcracks in some of the grains and inferred that the low temperature regime was dominated by semi-brittle deformation. At high temperatures, they observed the grains to be flattened and grain boundaries were irregular, whereas at mid-temperature no elongation or flattening of grains was observed. Samples deformed at mid- and high-temperature had <0.05 vol% and 0.1–2.5 vol% melt, respectively, and indicated grain boundary migration recrystallization as the deformation mechanism. When the rock is a mixture of minerals feldspar and pyroxene, the feldspar rheology dominates if pyroxene content is less than 50%. Hence, we refer to feldspar in the introduction and discussion section, and refer as granulite when discussing about data and results.

3. Method

The steady-state creep mainly depends on the external variables such as temperature, pressure, and stress (as discussed above). However, the transient creep on the other hand, in addition to external variables depend on the intrinsic variables such as internal stress. Internal stress arises due to evolution of microstructures such as dislocation density and/or grain size (e.g., S. Karato, 2008). Therefore, while the steady-state depends on the applied stress, the transient creep depends on the effective stress, which is less than the applied stress. In order to capture this kind of behavior, two theoretical models have been proposed in olivine that is, intergranular (S. Karato, 1998; Masuti & Barbot, 2021) and intragranular (Hansen et al., 2019). In this study, we consider a nonlinear Burgers model, in which, the dashpot of the Kelvin element represents a soft slip system and dashpot of the Maxwell element represents a hard slip system, and hence captures the intergranular model. In this model, the transient creep flow law is given by

$$\dot{\varepsilon}_{\mathrm{K}} = A_{\mathrm{K}} q_{\mathrm{K}} \|q_{\mathrm{K}}\|^{n_{\mathrm{K}}-1} d^{-p_{\mathrm{K}}} \exp\left(-\frac{E_{\mathrm{K}}}{RT}\right), \tag{2}$$

where the form $q\,\|q\|^{n-1}$ is to allow retrograde deformation in the Kelvin dashpot. A_{K}, n_{K}, p_{K}, and E_{K} are similar to Equation 1 but represent the transient creep flow law parameters, and the effective stress (q_{K}) is

$$q_{\mathrm{K}} = \sigma - G_{\mathrm{K}} \varepsilon_{\mathrm{K}}, \tag{3}$$

where ε_{K} is the cumulative strain in the Kelvin element and G_{K} is a work-hardening coefficient. The steady-state strain rate, which is represented by Maxwell element, is given by Equation 1. The total strain rate ($\dot{\varepsilon}$) in the Burgers model is the sum of elastic and inelastic component. Using Hooke's law ($\varepsilon = \sigma/G$), we can write the stress rate as

$$\dot{\sigma} = G_{\mathrm{M}}\left(\dot{\varepsilon} - \dot{\varepsilon}^{i}\right), \tag{4}$$

where $\dot{\varepsilon}^{i}$ is the total inelastic strain rate in the Burgers model and is equal to the sum of strain rate in the Kelvin and Maxwell elements (i.e., $\dot{\varepsilon}_{\mathrm{K}} + \dot{\varepsilon}_{\mathrm{ss}}$) and G_{M} is the Young's modulus. The detailed description of the model used to estimate the flow law parameters have been discussed in Masuti and Barbot (2021) and also discussed in Supporting Information S1.

Using a Markov chain Monte Carlo (MCMC) method, we obtained the flow law parameters for both quartz and granulites from the experimental data. The approach is described in Masuti and Barbot (2021). The MCMC method is slightly different from the classical Gibbs sampling (see Figure S2 in Supporting Information S1). Gibbs sampling for a nonlinear problem involves mainly two steps. First, we need to determine the conditional probability density function (PDF) of a chosen dimension, while the other dimensions are fixed. Second, drawing a random sample from the conditional PDF determined in the first step. Although the Gibbs sampling is very efficient, the first step is time consuming depending on the number of random samples required to estimate the full

Table 1
Flow Law Parameters of Quartz Aggregates Estimated From the Constant Strain Rate Experimental Data of Gleason and Tullis (1995)

Parameter	Symbol	Value	Bounds	Unit	Study
Pre-exponential factor	A_K	$10^{-6.53\pm0.2}$	10^{-9}–10^{6}	$s^{-1}MPa^{-n_K}$	This study
Hardening coefficient	G_K	600 ± 41	0.1–10^4	MPa	This study
Stress exponent	n_K	2.0 ± 0.06	0.01–5	–	This study
Activation energy	E_K	67 ± 4	30–600	kJ/mol	This study
Young's modulus	G_M	18.6 ± 0.1	1–100	GPa	This study
Pre-exponential factor	A_{ss}	$10^{-4.8\pm0.03}$	10^{-9}–10^{6}	$s^{-1}MPa^{-n_{ss}}$	This study
Stress exponent	n_{ss}	4.0 ± 0.9	–	–	Gleason and Tullis (1995)
Activation energy	E_{ss}	220 ± 56	–	kJ/mol	Gleason and Tullis (1995)

Note. The errors are for one standard deviation for all the uncertainties reported in this study.

conditional PDF. In order to reduce the computational time, instead of determining the exact conditional PDF, we draw 1000 random samples in the chosen dimension while keeping the other dimension fixed and compute the likelihood for each sample. In the next step, we choose the sample with highest likelihood as the accepted sample. By doing so, we do not need to know the exact conditional PDF of the current dimension.

We assume the starting (i.e., proposal) distribution for the MCMC to be uniformly distributed within a wide range of bounds for the flow parameter (Tables 1–4). The bounds are chosen based on previous studies of steady-state parameters (e.g., Hirth et al., 2001; Luan & Paterson, 1992; Rutter & Brodie, 2004; Rybacki & Dresen, 2000; Tokle et al., 2019) and sometimes vary over several orders of magnitude. For example, the pre-exponential factor bounds are from 10^{-9} to 10^{6} $s^{-1}MPa^{-n_K}$. If the posterior distributions for any parameter are skewed, the MCMC inversion was carried out widening these bounds for a couple of orders of magnitude. The process of increasing the bounds was carried out until we obtain the decent Gaussian distribution for each parameter. For each inversion, similar to Masuti and Barbot (2021), a total of 2×10^5 samples were generated. In the post-processing step, we discard the initial 10^4 samples and from the remaining samples we retain every 100th sample to plot joint and marginal posterior distribution of the model parameters (i.e., A_K, n_K, G_K, E_K, A_{ss}, and G_M).

4. Flow Law Parameters

All joint and marginal posterior distributions of the model parameters for quartz are shown in Figure 1 and for granulite in Figures 3 and 4 at mid and high temperature conditions, respectively. All marginal distributions are approximately Gaussian and we conclude that the model parameters (i.e., A_K, n_K, G_K, E_K, A_{ss}, and G_M) are well constrained. Using the mean values of these distributions, the best fit model parameters were used to calculate stress-strain curves in comparison to the measured data for quartz (Figure 2) and granulite (Figures 5 and 6), showing in most cases excellent agreement, except at $T = 1050$°C for quartz and at $T = 1150$°C for granulite.

4.1. Quartz

Gleason and Tullis (1995) determined a stress exponent of $n_{ss} \sim 4$ and an activation energy of $E_{ss} \sim 220$ kJ/mol for dislocation creep of quartz under melt free conditions in the steady-state regime, based on constant strain rate tests performed at ~1.5 GPa confining pressure, temperatures between 1000 and 1100°C and axial strain rates of 1.5×10^{-6} to 7.5×10^{-5} s^{-1}. Measured creep stresses were in the range between ~70 and ~230 MPa (Figure 2). Keeping these steady-state values fixed, we estimated a stress exponent of $n_K \sim 2$ and an activation energy of $E_K \sim 67$ kJ/mol for the transient creep of quartz (Table 1; Table S1 in Supporting Information S1). The stress exponent and activation energy of transient creep are lower than those of steady-state creep. The estimated steady-state activation energy of wet quartz in the dislocation creep regime has been controversial within different studies, resulting in a wide range of values. These values may be separated into two categories. In the first category, some studies estimated E_{ss} to be ~200 kJ/mol (e.g., Gleason & Tullis, 1995; Richter et al., 2018; Rutter & Brodie, 2004). Other studies found the activation energy to be smaller with $E_{ss} \sim 120$ kJ/mol (e.g., Hirth et al., 2001; Luan & Paterson, 1992). Recently, most of the published

Table 2
Same as Table 1 Except That the Steady-State Parameters We Used Are From Tokle et al. (2019)

Parameter	Symbol	Value	Bounds	Unit	Study
Pre-exponential factor	A_K	$10^{-5.3\pm0.3}$	10^{-9}–10^{6}	$s^{-1}MPa^{-n_K}$	This study
Hardening coefficient	G_K	660 ± 60	0.1–10^4	MPa	This study
Stress exponent	n_K	1.82 ± 0.14	0.01–5	–	This study
Activation energy	E_K	87 ± 10	30–600	kJ/mol	This study
Young's modulus	G	18.6 ± 0.1	1–100	GPa	This study
Pre-exponential factor	A_{ss}	$10^{-8.0\pm0.04}$	10^{-9}–10^{6}	$s^{-1}MPa^{-n_{ss}}$	This study
Stress exponent	n_{ss}	4.0 ± 0.3	–	–	Tokle et al. (2019)
Activation energy	E_{ss}	140 ± 56	–	kJ/mol	Tokle et al. (2019)

data was revisited and it has been suggested that the high activation energy of ∼200 kJ/mol is obtained by assuming the stress exponent n_{ss} to be same for low and high flow stresses (Tokle et al., 2019). The authors suggested different stress exponents of 3 and 4, and activation energy of 105 kJ/mol and 140 kJ/mol for high (>250 MPa) and low flow stress, respectively, possibly induced by a change of dominant slip systems (Tokle et al., 2019). To verify that the transient creep parameters are not biased by the assumed steady-state parameters, we conducted a second inversion run assuming the steady-state activation energy to be E_{ss} = 140 kJ/mol and stress exponent to be n_{ss} = 4 (following Tokle et al. (2019) flow law parameters) as the measured stress are well below 250 MPa (Figure 2). Under these assumptions, the activation energy and stress exponent we get for the transient creep are $E_K \sim 87$ kJ/mol and $n_K \sim 1.8$, respectively, which are again distinctly lower than their steady state counterparts (Table 2).

We find quite similar hardening coefficients of $G_K \sim 600$ MPa and Young's moduli of $G_M \sim 18$ GPa in both inversions. The pre-exponential factor A_K for transient creep of quartz aggregates is $10^{-6.53}$ $s^{-1}MPa^{-n_K}$, whereas the pre-exponential factor for the steady-state creep is A_{ss} is $10^{-4.8}$ s^{-1} $MPa^{-n_{ss}}$, which is within the uncertainties of $1.1 \times 10^{(-4\pm2)}$ s^{-1} $MPa^{-n_{ss}}$ (Gleason & Tullis, 1995). When using steady-state parameters from Tokle et al. (2019), the pre-exponential term for transient creep is $10^{-5.3\pm0.3}$ s^{-1} MPa^{-n_K}, and for steady-state creep it is $10^{-8.0\pm0.04}$ s^{-1} $MPa^{-n_{ss}}$, whereas the steady-state pre-exponential factor reported by Tokle et al. (2019) is 8×10^{-12} MPa^{-n} s^{-1} without any uncertainties. There are 14 stress versus strain curves available from Gleason and Tullis (1995). The fit is satisfactory for most of the stress versus strain curves except a couple at 1000°C, $10^{-5.8}$ s^{-1} and 1050°C, $10^{-5.8}$ s^{-1} (Figures 2a and 2k). The misfit between the data and model of 1000°C, $10^{-5.8}$ s^{-1} (Figure 2a) is within the stress resolution of molten salt assembly (Holyoke III & Kronenberg, 2010) and at 1050°C, $10^{-5.8}$ s^{-1} strain weakening was observed. The small misfit between measured and modeled data may arise from the fact that in our inversion each data point in all stress versus strain curves is given equal weight, which will reduce the influence of low stress data compared to high stress data in minimizing the global misfit.

4.2. Granulite

Since our main aim here is to determine the flow law parameters of transient creep in the fully plastic regime, we analyzed only mid and high temperature data from Zhou et al. (2017) ignoring the low-temperature data, where deformation is in the semi-brittle regime. We apply the same method as described in the above paragraph for quartz data. For steady-state creep, Zhou et al. (2017) determined stress exponents of n_{ss} = 5.7 ± 0.1 and 4.8 ± 0.1, and activation energies of E_{ss} = 525 ± 34 kJ/mol and 1392 ± 63 kJ/mol for mid- and high-temperature data, respectively. In our simulations, we use the stress exponent and activation energy of steady-state creep from Zhou et al. (2017) obtained at mid-temperature conditions (Table 3). Our fitted stress exponent for transient creep in the mid-temperature regime is close to 1 (n_K = 0.9 ± 0.1) and the activation energy is E_K = 281 ± 30 kJ/mol (Table 3, Figure 3; Table S2 in Supporting Information S1). For high temperature conditions, the activation energy of ∼1,392 kJ/mol determined by Zhou et al. (2017) is much higher than any of the previous studies (e.g., Chen et al., 2021; Rybacki & Dresen, 2000). Hence, we use the stress exponent of $n_{ss} \sim 3.0$ and activation energy of $E_{ss} \sim 360$ kJ/mol from Rybacki and Dresen (2000) for dislocation creep of anorthite aggregates (Table 4). The best fit stress exponent in the transient regime is then n_K = 1.0 ± 0.1 and the corresponding activation energy is E_K = 218 ± 38 kJ/mol (Table 4, Figure 4; Table S3 in Supporting Information S1). For comparison, we also

Table 3
Flow Law Parameters of Feldspar for the Mid-Temperature (1050–1100°C) Conditions Estimated From the Granulites Data of Zhou et al. (2017)

Parameter	Symbol	Value	Bounds	Unit	Study
Pre-exponential factor	A_K	$10^{4.19\pm0.96}$	10^{-12}–10^{10}	$s^{-1}MPa^{-n_K}$	This study
Hardening coefficient	G_K	7.0 ± 0.6	1–100	GPa	This study
Stress exponent	n_K	0.9 ± 0.1	0.01–10	-	This study
Activation energy	E_K	281 ± 30	30–1,000	kJ/mol	This study
Young's modulus	G	14.0 ± 0.6	1–100	GPa	This study
Pre-exponential factor	A_{ss}	$10^{1.09\pm0.02}$	10^{-12}–10^{12}	$s^{-1}MPa^{-n_{ss}}$	This study
Stress exponent	n_{ss}	5.7 ± 0.1	–	–	Zhou et al. (2017)
Activation energy	E_{ss}	525 ± 34	–	kJ/mol	Zhou et al. (2017)

conducted an experiment with the steady-state creep parameters from Zhou et al. (2017) (i.e., n_{ss} = 4.7 and n_{ss} = 1392 kJ/mol) for the high temperature data, resulting in n_K = 2.3 and E_K = 570 kJ/mol, which are much higher than using the steady state n_{ss} and E_{ss} data from Rybacki and Dresen (2000). Evidently, in both temperature regimes the stress exponents and activation energies for transient creep are clearly lower than those for steady state creep, similar to quartz.

Zhou et al. (2017) conducted two experiments at mid-temperatures of 1050 and 1100°C, and three experiments at high-temperatures of 1125, 1140, and 1150°C. Using our inversion results, we could successfully fit both mid- and high-temperature stress versus strain curves (Figures 5 and 6). As explained above for quartz, there is a small misfit between data and model, in particular for the data at 1150°C (Figure 6). The estimated pre-exponential factor are $10^{4.2\pm0.9}$ $s^{-1}MPa^{-n_K}$ and $10^{1.09\pm0.02}$ $s^{-1}MPa^{-n_{ss}}$ for transient and steady-state creep at mid-temperatures (Table 3), and $10^{2.03\pm1.41}$ $s^{-1}MPa^{-n_K}$ and $10^{2.24\pm0.07}$ $s^{-1}MPa^{-n_{ss}}$ at the high-temperatures, respectively (Table 4). The hardening coefficient and Young's modulus for mid-temperature are G_K = 7 ± 0.6 GPa and 14 ± 0.6 GPa, and for high-temperature they are 2.63 ± 0.3 GPa and 6.0 ± 0.3 GPa, respectively. These hardening coefficients and Young's moduli are smaller than the independent estimates of ∼100 GPa and ∼40 GPa for plagioclase feldspar aggregates (Pabst et al., 2015).

5. Discussion

Most strikingly, our results indicate a systematically lower stress exponent and activation energy for transient dislocation creep of quartz and granulite compared to steady state creep. Similar results have been obtained for olivine aggregates, the major upper mantle mineral (Masuti & Barbot, 2021) and the results have been explained by extending the theoretical model of jogs (e.g., S. Karato, 2010; Masuti et al., 2019). We briefly describe the jog model in the following paragraph.

Table 4
Flow Law Parameters of Feldspar for the High-Temperature Conditions (1125–1150°C) Estimated From the Granulites Data of Zhou et al. (2017)

Parameter	Symbol	Value	Bounds	Unit	Study
Pre-exponential factor	A_K	$10^{2.03\pm1.41}$	10^{-12}–10^{10}	$s^{-1}MPa^{-n_K}$	This study
Hardening coefficient	G_K	2.63 ± 0.3	1–100	GPa	This study
Stress exponent	n_K	1.0 ± 0.1	0.01–10		This study
Activation energy	E_K	218 ± 38	30–1,000	kJ/mol	This study
Young's modulus	G	6.0 ± 0.3	1–100	GPa	This study
Pre-exponential factor	A_{ss}	$10^{2.24\pm0.07}$	10^{-12}–10^{12}	$s^{-1}MPa^{-n_{ss}}$	This study
Stress exponent	n_{ss}	3.0 ± 0.3	–	–	Rybacki and Dresen (2000)
Activation energy	E_{ss}	360 ± 10	–	kJ/mol	Rybacki and Dresen (2000)

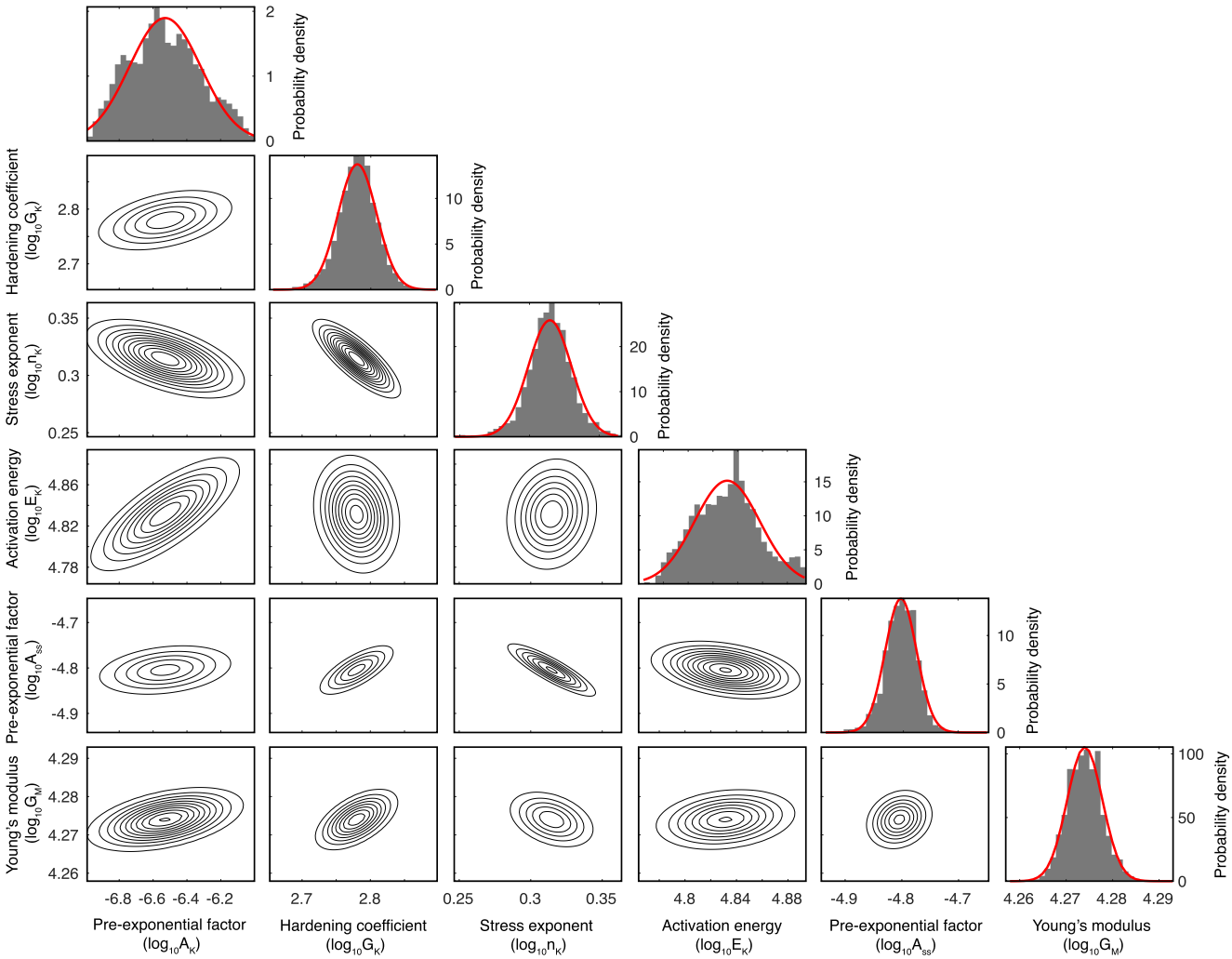

Figure 1. MCMC simulation results for quartz. From the simulation samples, we plot the histograms and contour plots for the flow law parameters of the transient creep of quartz under wet conditions. These histograms and contour plots represent the marginal and joint distributions, respectively. There is strong correlation between stress exponent (n_K) and the hardening coefficient (G_K), and also between activation energy (E_K) and pre-exponential factor (A_K). There is a weak correlation between pre-exponential coefficients of transient (A_K) and steady-state (A_{ss}).

In the dislocation creep regime, the deformation rate is controlled by the slowest diffusing element and the jog density for olivine aggregates (e.g., S. Karato, 2010). Masuti and Barbot (2021) extended this model to explain the difference in activation energies of transient and steady-state creep in the dislocation regime. The authors proposed that the activation energy of dislocation creep depend on the diffusion process and jog density. Furthermore, they found that the activation energy for diffusion of Si, which is the slowest diffusing element, in olivine under dry conditions matches with the activation energy of transient dislocation creep in olivine aggregates. For olivine, the activation energy for steady-state creep is higher than for transient creep. Based on these findings, the authors proposed that the activation energy of dislocation creep is the sum of activation energy of the slowest diffusing element and the activation energy of jog formation that is,

$$E_{\text{creep}} = E_{\text{D}} + E_{\text{j}}, \tag{5}$$

where E_{creep} is the activation energy of dislocation creep, E_{D} is the activation energy of the slowest diffusing element, and E_{j} is the jog formation energy. For polycrystalline materials, where individual crystals may exhibit highly anisotropic properties, Masuti et al. (2019) proposed that the soft slip system, which is likely saturated with jogs, dominates the deformation behavior during transient creep. Since the soft slip system is almost saturated with jogs, jog formation energy is low in the transient regime ($E_{\text{j}} \approx 0$), hence the activation energy of the

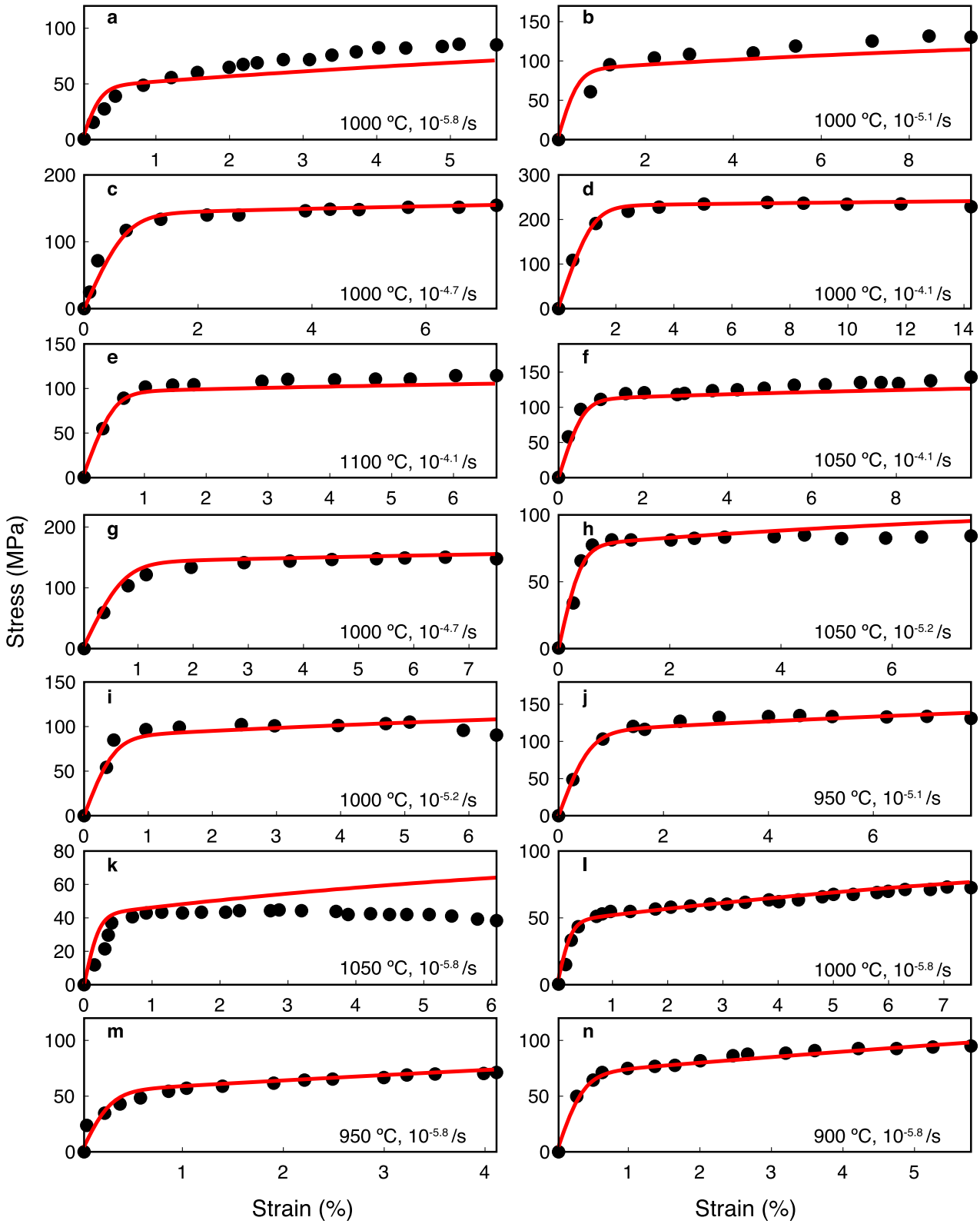

Figure 2. Quartz mechanical data (black dots) and the best fit model (red line). Red line represents one of the many fits that could be plotted from the posterior distribution. The fit to most of the data is fine except for 1000°C, $10^{-5.8}$ s^{-1} and 1050°C, $10^{-5.8}$ s^{-1}.

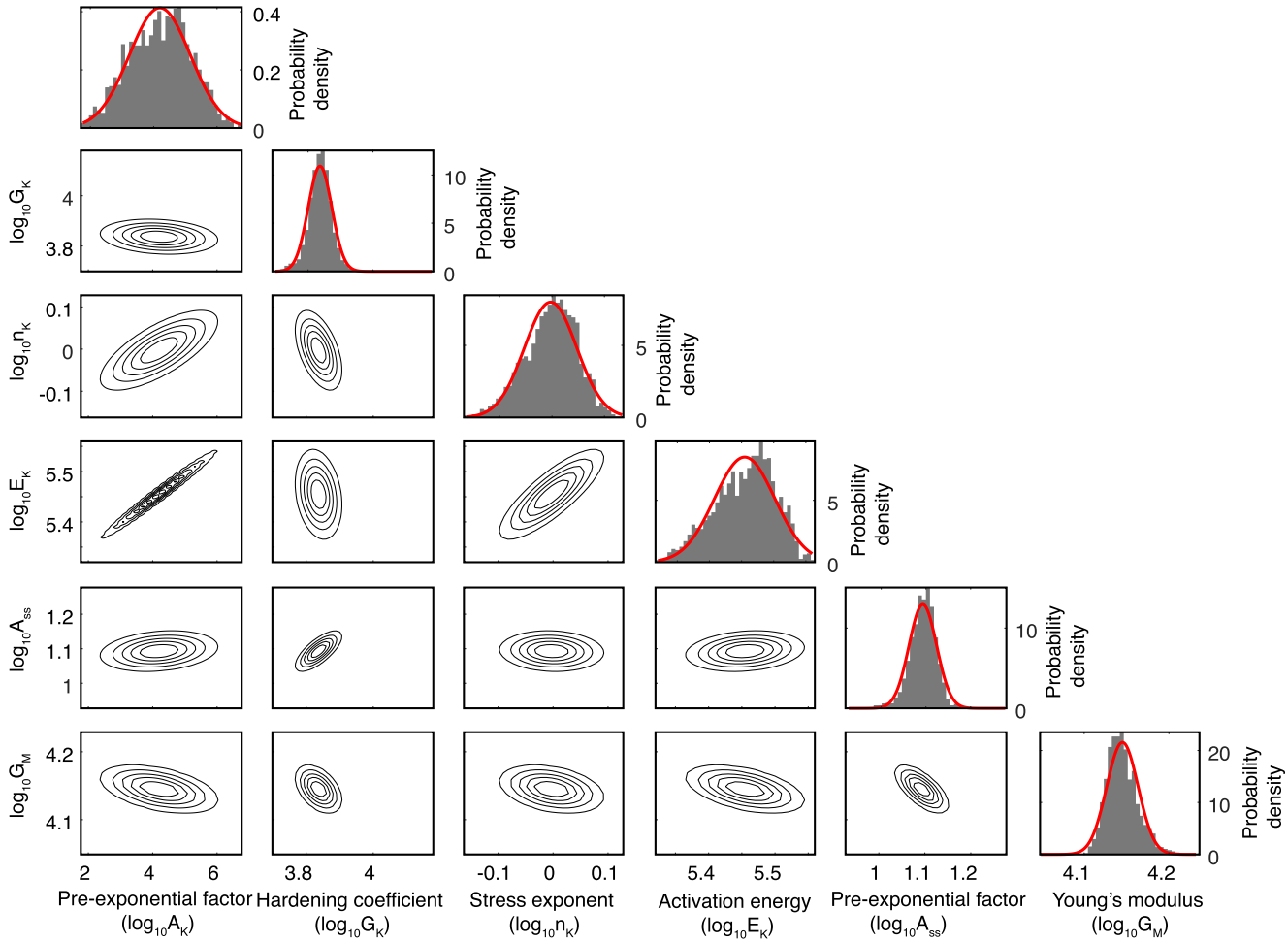

Figure 3. MCMC simulation results for feldspar under mid-temperature (1050–1100°C) conditions. Similar to quartz, there is a weak correlation between A_K and A_{ss}. However, there is strong correlation between the stress exponent (nK) and the activation energy (E_K), which is not the case for quartz.

transient creep is equal to the activation energy of the slowest diffusing species and as Si is assumed to be the slowest diffusing element in olivine (Weertman, 1968; Kohlstedt, 2006; S. Karato, 2010):

$$E_{\text{transient}} = E_{\text{creep}} = E_{\text{D}} \approx E_{\text{Si}}. \tag{6}$$

On the other hand, the hard slip system, which is unsaturated with jogs, dominates during steady-state creep, for which the jog formation energy is high (i.e., $E_j > 0$)

$$E_{\text{ss}} = E_{\text{creep}} = E_{\text{D}} + E_{\text{j}} > E_{\text{transient}}. \tag{7}$$

In order to check whether this model is applicable to quartz and feldspar, we need two things. First, we need information about the dominant slip systems during deformation of the mineral. Second, we need to know the activation energy of the slowest diffusing element in the mineral. In the following paragraphs, we discuss the slip systems and activation energies of quartz and feldspar.

5.1. Transient Creep of Quartz

There are several slip systems in quartz that may contribute to the deformation of polycrystalline quartz. The dominant slip system, which contributes significantly to deformation, depends on temperature (e.g., Tullis et al., 1973), pressure (e.g., Kronenberg & Tullis, 1984), and water content (e.g., Griggs, 1967). The dominant slip system changes from basal <a> to prism [c] depending on temperature (Okudaira et al., 1995), water content (e.g., Griggs & Blacic, 1965), and stress (e.g., Tokle et al., 2019). In order to understand the deformation behavior

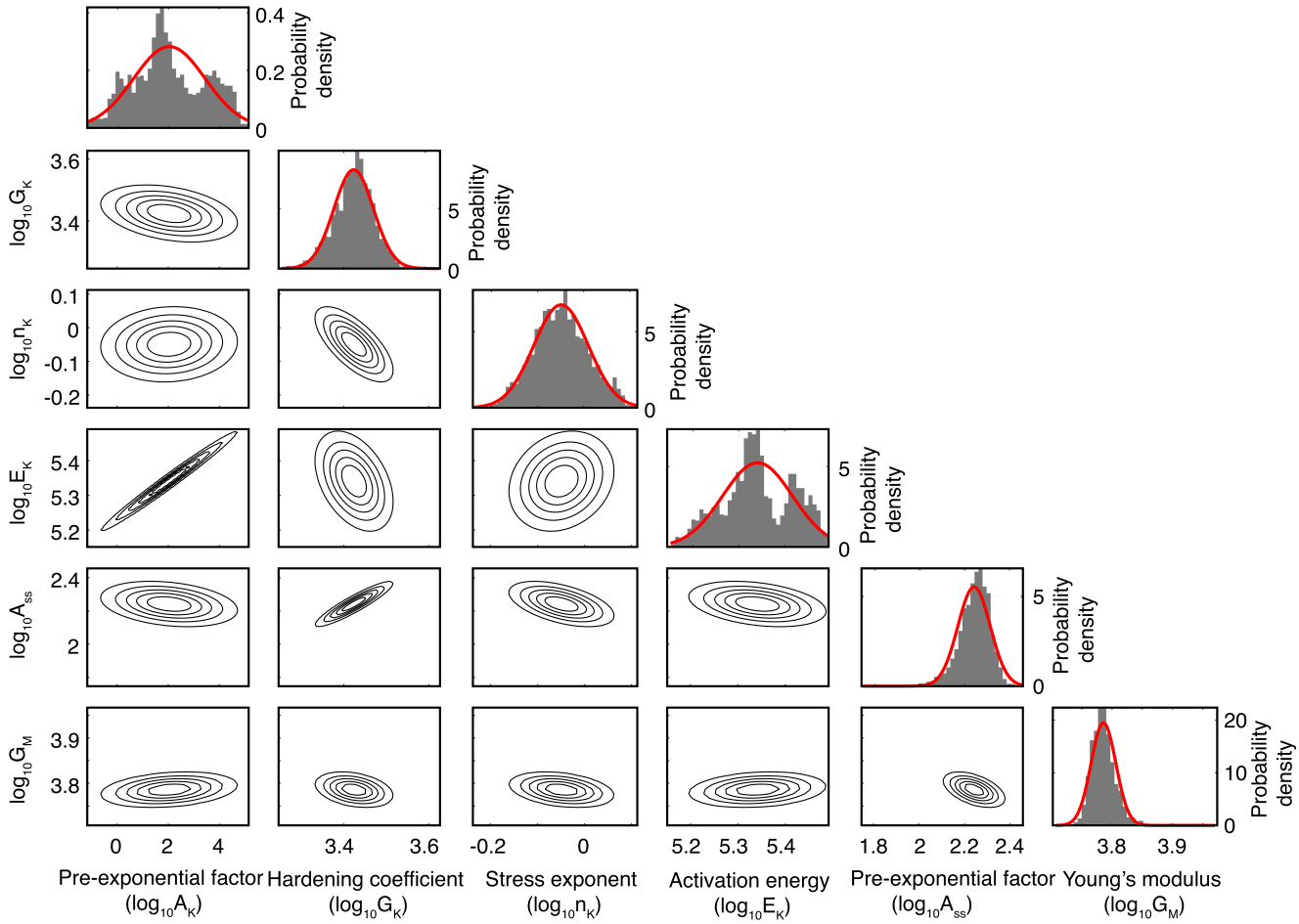

Figure 4. MCMC simulation results for feldspar under high-temperature (1125–1150°C) conditions. The marginal density of the activation energy (E_K) is a bimodal distribution with the mode matching the mean of the distribution but there is a second peak at 260 kJ/mol.

of individual slip systems in quartz, several single crystal experiments have been conducted (e.g., Christie et al., 1964; Linker et al., 1984; Muto et al., 2011).

Griggs and Blacic (1965) reported that the dominant slip system changes from basal slip to prismatic slip above 750°C. More recently, Muto et al. (2011) conducted single crystal study with the goal of activating the basal <a>, prism <a>, and prism [c] slip and showed that the basal <a> system is weaker than the prism [c] system at high temperatures of ~900°C and confining pressure of 1.5 GPa. In addition, the authors concluded that the quartz aggregate strength is controlled by the hardest slip system (i.e., prism [c]) under steady-state conditions (Muto et al., 2011). Therefore, we propose that the easy basal slip system dominates the transient creep of quartz aggregates under high temperature conditions, which may have an impact on the prevailing activation energy and stress exponent. This interpretation is relevant for the thermodynamic conditions applied in the experiments by Gleason and Tullis (1995). However, the easy/hard slip system in the transient and steady-state creep regimes may change in nature as the water content, temperature, and pressure change with depth as shown in the case of olivine (e.g., Jung & Karato, 2001; Masuti et al., 2019; Raterron et al., 2009).

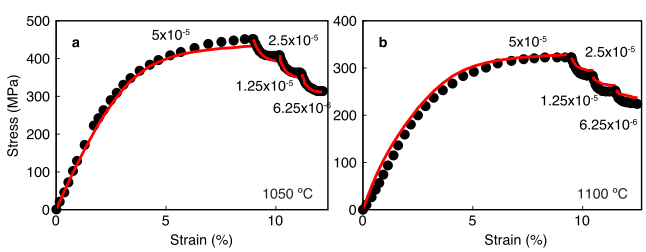

Figure 5. Best fit model with stress versus strain series data (black dots) for feldspar under mid-temperature conditions.

For a number of silicates including quartz, both grain boundary diffusion and volume diffusion rates of many species have been determined (see Brady, 1995, for a review). For quartz, the activation energy of Si for volume diffusion is 734 kJ/mol (Béjina & Jaoul, 1996) and for grain boundary diffusion it is 178 ± 38 kJ/mol under dry conditions (Farver & Yund, 2000). Based

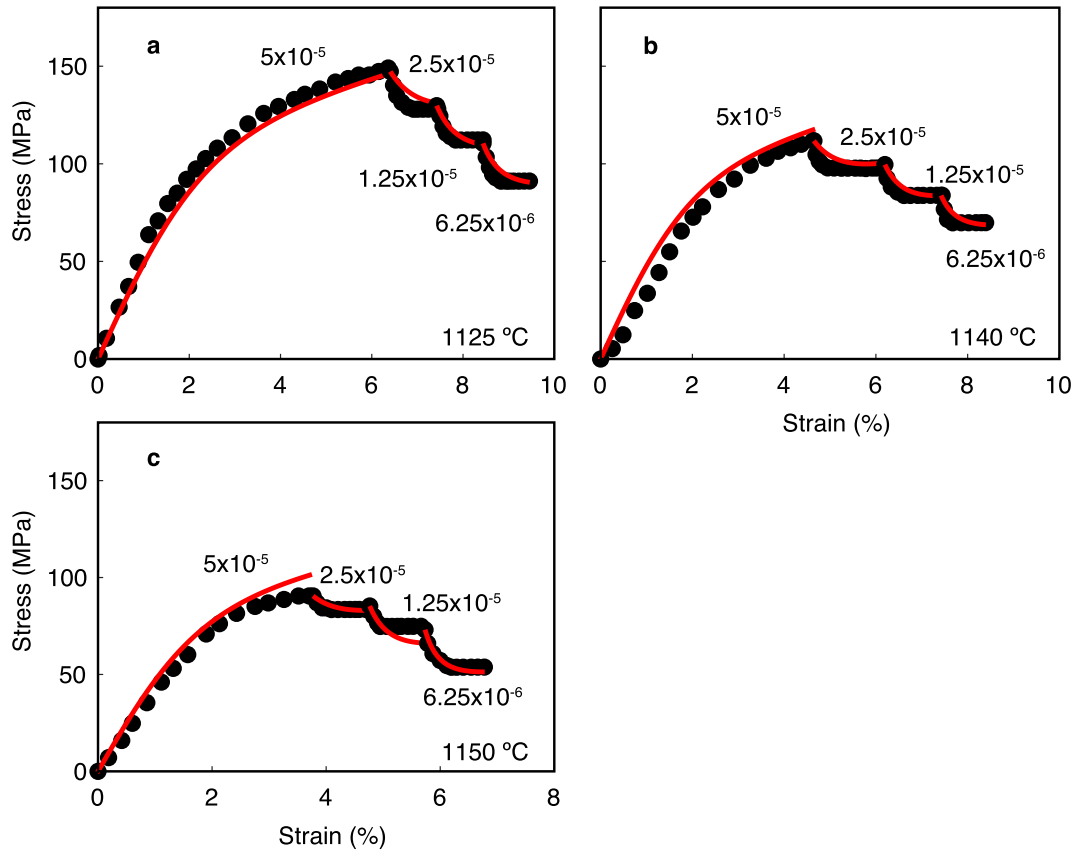

Figure 6. Best fit model with stress versus strain series data (black dots) for strain rate-stepping experiments on feldspar at high-temperature conditions.

on these results, silicon has been established to be the slowest diffusing and rate controlling species in quartz (Farver & Yund, 2000). It is well known that water significantly reduces the strength of quartz and the activation energy of Si for grain boundary diffusion under wet condition at 150 MPa confining pressure is found to be ~137 ± 18 kJ/mol (Farver & Yund, 2000). In addition, Farver and Yund (2000) showed that the silicon diffusion rate at 150 MPa confining pressure under wet condition is 10 times higher than at atmospheric pressure and dry condition. The effect of pressure is often ignored in these diffusion studies. However, the effect of pressure under wet conditions is non-monotonic due to the water fugacity term and the activation volume of diffusion. Here, we speculate that the activation energy of silicon diffusion under high pressure of ~1,500 MPa (i.e., confining pressure used in Gleason and Tullis (1995) experiments) may be lower than ~110 kJ/mol (assuming an activation volume of 15 cm^3/mol). The activation energy that we estimate for the transient creep of quartz is ~67 ± 4 and ~87 ± 10 kJ/mol, depending on the input parameters for n_{ss} and E_{ss} (Tables 1 and 2). These values are close to the estimated activation energy of silicon diffusion in quartz (~110 kJ/mol). Based on the plastic anisotropy observed in single crystal studies (Muto et al., 2011) and the agreement of the activation energy of transient creep with that of silicon grain boundary diffusion, we propose that the basal slip system, which likely dominates during transient creep, is saturated with jogs. Therefore, the jog model explained above for olivine aggregates is also applicable for quartz.

5.2. Transient Creep of Feldspar/Granulite

The granulite data analyzed here originate from samples that contained ~50% plagioclase and ~40% pyroxene. A detailed experimental study on high temperature creep of feldspar/pyroxene mixtures demonstrated that the feldspar rheology dominates the overall behavior if the pyroxene content is less than or equal to ~50% (Dimanov & Dresen, 2005). Therefore, we discuss the results assuming that feldspar rheology dominates under the current conditions and the effect of pyroxene is negligible.

Among the several slip systems available in feldspar, slip on (010)[001], (001)1/2 <110>, {001} <100>, (010)[100], and {111}1/2 <110> systems are reported (Montardi & Mainprice, 1987; Passchier & Trouw, 2005). At high temperatures, (010)[001] was considered as the dominant slip system in experimentally and naturally deformed feldspar samples (Ji et al., 1988; Kruhl, 1987; Olsen & Kohlstedt, 1984; Stünitz et al., 2003). However, more recently (010)[100] and/or (001)[100] slip systems have been proposed as dominant slip systems during creep (Ji et al., 2004; Mehl & Hirth, 2008). In order to determine the easy and hard slip systems, one has to conduct deformation experiments on single crystal feldspar by activating the specific slip system and determine the strength of the slip system. To our best knowledge, there are no deformation studies aiming to activate specific slip system conducted so far.

We find that the activation energy of transient creep for feldspar at mid- and high-temperature conditions to be 281 kJ/mol and 218 kJ/mol, respectively. In order to verify if the theoretical model of jogs is applicable or not, we need to know the activation energy of Si diffusion in feldspar. Activation energy of Si diffusion in feldspar under dry conditions is ~465 ± 50 kJ/mol (Cherniak, 2003). However, the mechanical data from Zhou et al. (2017) we use for modeling were conducted under hydrous conditions and to our best knowledge, no experimental studies exist to determine the activation energy of Si diffusion in feldspar under hydrous conditions. On the other hand, based on the disordering kinetics of Al/Si in feldspar, the activation energy of Si diffusion is suggested to be ~270 kJ/mol (Yund & Tullis, 1980), which is within the uncertainties of the activation energy of transient creep we estimated for the mid- and high-temperature conditions. Although the dominant slip system for the transient and steady-state creep is not established in case of feldspar, we propose that the jogs model may still be applicable to feldspar based on the similarity of the activation energy of diffusion of Si in feldspar and the activation energy of transient creep.

5.3. Low Stress Exponent of the Transient Creep in Both Quartz and Feldspar

Steady-state strain rate is given by Orowan's equation:

$$\dot{\varepsilon} = \rho b v, \tag{8}$$

where ρ is the dislocation density, b is the Burgers vector, and v is the dislocation velocity. The power law stress dependency of strain rate mainly comes from the dependency of dislocation density and dislocation velocity on stress (see Kohlstedt, 2006, and references there in for more details). At steady-state, dislocation velocity depends linearly on the stress and the relation between dislocation density (ρ) and stress (σ) is of the form:

$$\rho \propto \sigma^m. \tag{9}$$

The theoretical value of exponent (m) is considered to be 2, while a range of values from 1.4 to 2 have been reported for different materials (e.g., Poirier, 1985; S. Karato & Jung, 2003). Hence, dislocation creep has a power law relationship between strain rate and stress at steady-state. However, during transient creep the dislocation density is not constant, and both stress and dislocation density are low compared to their values at steady-state. Under such conditions, it has been proposed that the dislocation density is weakly dependent on the stress (e.g., Mulyukova & Bercovici, 2022; Poirier, 1985). Therefore, the stress exponent of transient creep in silicate minerals is expected to be lower than for steady-state creep.

Quartz and feldspar are the most abundant minerals in the continental crust, and olivine is most abundant in both continental and oceanic upper mantle. In this study, we find that the stress exponent and activation energy of transient creep for quartz and feldspar are smaller than those for steady-state creep. These results are consistent with results for olivine (Masuti & Barbot, 2021), a dominant upper mantle mineral. Based on these results, we propose that the stress exponent and activation energy of transient creep are smaller than for steady-state creep for all volumetrically important silicate minerals of the crust and upper mantle.

5.4. Implication for Postseismic Deformation

Using the flow law parameters derived for wet feldspar (Table 4), we estimate the stress versus time evolution for different strain rate conditions (Figure 7). Although transient creep is not sensitive to the background stress, steady-state creep depends on background stress (Masuti et al., 2016). Therefore, we first run a forward model for a duration of 300 years at a strain rate of 5×10^{-14} s^{-1}, which is the approximate strain rate at ~30 km depth and

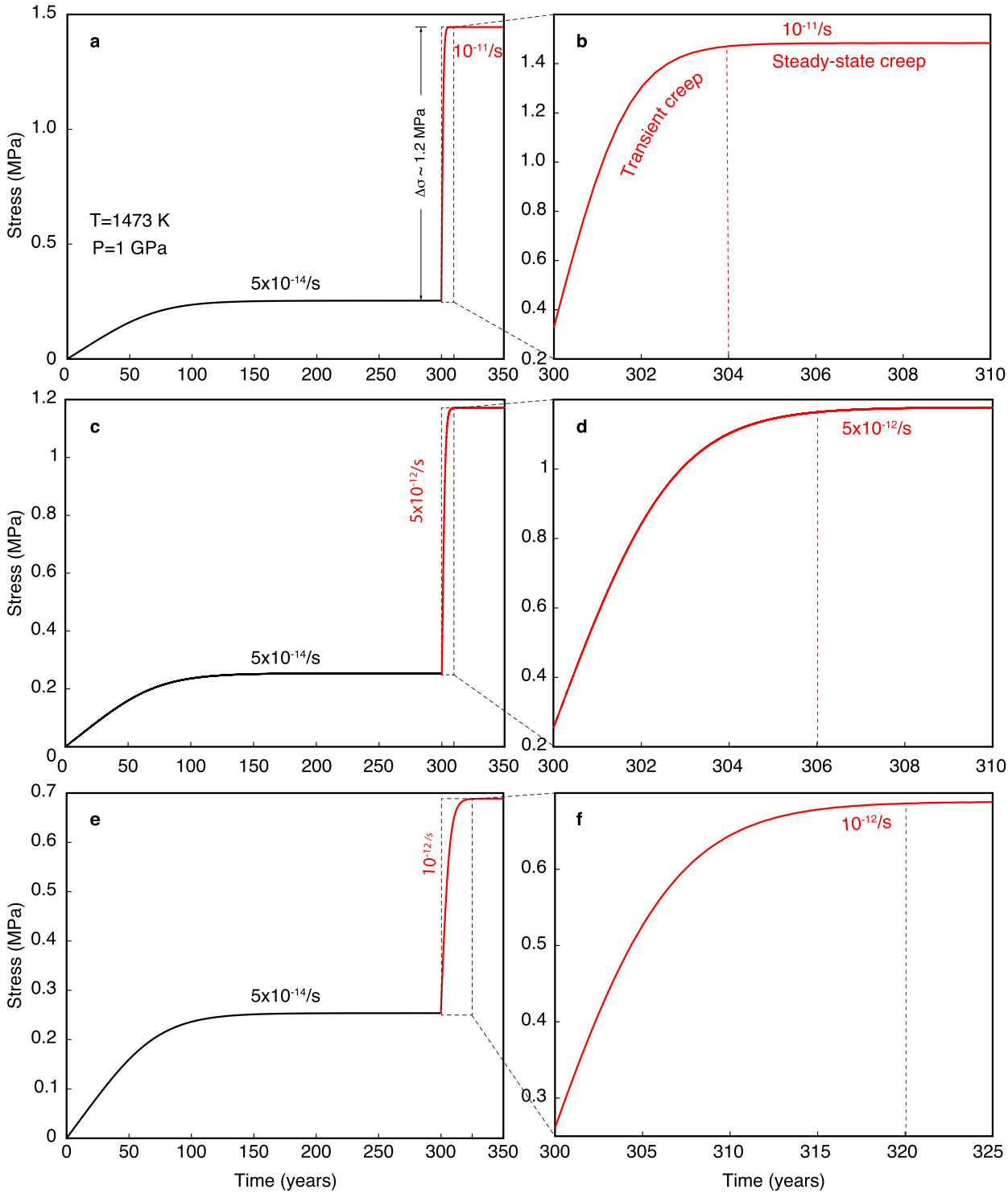

Figure 7. Stress versus time estimates using the flow law parameters of granulite from Table 4. We assume the activation volume of transient and steady-state creep to be same as ~38 cm^3/mol (Rybacki et al., 2006). For all the simulations, the starting strain rate is same 5×10^{-14} s^{-1} and we increase the rate after reaching steady-state to check the approximate time needed to reach the steady-state from the perturbation. Figures on left (a, c, e) are full simulations and figures on right (b, d, f) are the zoomed in part to highlight the transient creep.

equivalent to a plate velocity of 5 cm/year at the surface. Once steady-state is achieved, we change the strain rate to faster rates of 10^{-11} s^{-1}, 5×10^{-12} s^{-1}, and 10^{-12} s^{-1} mimicking transient faster deformation rates immediately after an earthquake that are faster than the long-term tectonic strain rate. At a rate of 10^{-11} s^{-1} the associated

increase in stress is about 1.2 MPa to reach again steady state conditions (Figures 7a and 7b), which is equivalent to a stress change at ∼30–50 km depth after most of the large to great earthquakes (e.g., Freed, 2005). For a one half to one order of magnitude less change in strain rate, the stress perturbation decreases to ∼1 MPa and ∼0.5 MPa, respectively (Figures 7c–7f). From these calculations, we infer that after a large earthquake it probably takes a minimum of 4–6 years to reach steady-state conditions at the fastest rate (10^{-11} s^{-1}) and for the slowest strain rate of 10^{-12} s^{-1}, it may take much longer (about 20 years) to reach steady-state creep. Most postseismic studies have inferred that the transient creep is usually short-term process ∼1 year (e.g., Freed et al., 2012; Pollitz, 2005). However, from our simple simulations with laboratory derived flow law parameters, we conclude that transient creep may last longer than previously thought.

6. Conclusion

Using a MCMC approach and published mechanical data from previous studies conducted at constant strain rate, we estimated the transient creep flow law parameters of quartz and feldspar. The results suggest smaller activation energies and stress exponents than those of steady-state creep. We propose that the easy basal slip system dominates during the transient creep of quartz. However, due to lack of single crystal deformation studies in feldspar, the dominant easy slip system is not clear. Lower stress exponents of the transient (∼1–2) compared with steady-state creep could be due to the weak stress dependency of dislocation density in the transient regime. Based on the similarity of activation energies of transient creep and diffusion of Si in quartz and feldspar, we proposed that the theoretical model of jogs may be applicable to both quartz and feldspar. Our results are also consistent with the previously obtained results for transient creep of olivine aggregates, suggesting that the model assumptions are valid to the most abundant volumetrically important silicate minerals of the crust and uppermost mantle. Using the high-temperature feldspar flow law parameters and extrapolating to natural conditions, we suggest that deep in the crust transient creep dominates during the postseismic phase for a period of up to ∼20 years.

Data Availability Statement

All the data needed is available from original papers that is, Gleason and Tullis (1995) and Zhou et al. (2017), and also in digital form at Masuti et al. (2023a). The numerical code needed to reproduce the results are available at Masuti et al. (2023b).

Acknowledgments
SM was funded by JSPS Postdoctoral Fellowship for Research in Japan (standard) and Humboldt Research Fellowship for Postdoctoral Researchers. We thank the reviewers Andreas Kronenberg and Sascha Zertani for their constructive comments. We thank Douglas Schmitt for editorial handling.

References

Agata, R., Barbot, S. D., Fujita, K., Hyodo, M., Iinuma, T., Nakata, R., et al. (2019). Rapid mantle flow with power-law creep explains deformation after the 2011 Tohoku mega-quake. *Nature Communications*, *10*(1), 1–11. https://doi.org/10.1038/s41467-019-08984-7

Béjina, F., & Jaoul, O. (1996). Silicon self-diffusion in quartz and diopside measured by nuclear micro-analysis methods. *Physics of the Earth and Planetary Interiors*, *97*(1–4), 145–162. https://doi.org/10.1016/0031-9201(96)03137-8

Brady, J. B. (1995). Diffusion data for silicate minerals, glasses, and liquids. *Mineral Physics and Crystallography: A Handbook of Physical Constants*, *2*, 269–290.

Chen, J., Jin, Z., Liu, W., Wang, Y., & Zhang, J. (2021). Rheology of dry k-feldspar aggregates at high temperature and high pressure: An experimental study. *Tectonophysics*, *817*, 229072. https://doi.org/10.1016/j.tecto.2021.229072

Cherniak, D. (2003). Silicon self-diffusion in single-crystal natural quartz and feldspar. *Earth and Planetary Science Letters*, *214*(3–4), 655–668. https://doi.org/10.1016/s0012-821x(03)00394-7

Chopra, P. (1997). High-temperature transient creep in olivine rocks. *Tectonophysics*, *279*(104), 93–111. https://doi.org/10.1016/s0040-1951(97)00134-0

Christie, J., Griggs, D., & Carter, N. (1964). Experimental evidence of basal slip in quartz. *The Journal of Geology*, *72*(6), 734–756. https://doi.org/10.1086/627030

Deng, J., Gurnis, M., Kanamori, H., & Hauksson, E. (1998). Viscoelastic flow in the lower crust after the 1992 landers, California, earthquake. *Science*, *282*(5394), 1689–1692. https://doi.org/10.1126/science.282.5394.1689

Dhar, S., & Muto, J. (2023). Function model based on nonlinear transient rheology of rocks: An analysis of decadal GNSS time series after the 2011 Tohoku-Oki earthquake. *Geophysical Research Letters*, *50*(9), e2023GL103259. https://doi.org/10.1029/2023gl103259

Dhar, S., Muto, J., Ito, Y., Miura, S., Moore, J. D., Ohta, Y., & Iinuma, T. (2022). Along-arc heterogeneous rheology inferred from post-seismic deformation of the 2011 Tohoku-Oki earthquake. *Geophysical Journal International*, *230*(1), 202–215. https://doi.org/10.1093/gji/ggac063

Dhar, S., Muto, J., Ohta, Y., & Iinuma, T. (2023). Heterogeneous rheology of Japan subduction zone revealed by postseismic deformation of the 2011 Tohoku-Oki earthquake. *Progress in Earth and Planetary Science*, *10*(1), 1–27. https://doi.org/10.1186/s40645-023-00539-1

Diao, F., Xiong, X., & Wang, R. (2011). Mechanisms of transient postseismic deformation following the 2001 mw 7.8 kunlun (China) earthquake. *Pure and Applied Geophysics*, *168*(5), 767–779. https://doi.org/10.1007/s00024-010-0154-5

Dimanov, A., & Dresen, G. (2005). Rheology of synthetic anorthite-diopside aggregates: Implications for ductile shear zones. *Journal of Geophysical Research*, *110*(B7), B07203. https://doi.org/10.1029/2004jb003431

Dimanov, A., Dresen, G., Xiao, X., & Wirth, R. (1999). Grain boundary diffusion creep of synthetic anorthite aggregates: The effect of water. *Journal of Geophysical Research*, *104*(B5), 10483–10497. https://doi.org/10.1029/1998jb900113

Farver, J., & Yund, R. (2000). Silicon diffusion in a natural quartz aggregate: Constraints on solution-transfer diffusion creep. *Tectonophysics*, *325*(3–4), 193–205. https://doi.org/10.1016/s0040-1951(00)00121-9

Freed, A. M. (2005). Earthquake triggering by static, dynamic, and postseismic stress transfer. *Annual Review of Earth and Planetary Sciences*, *33*(1), 335–367. https://doi.org/10.1146/annurev.earth.33.092203.122505

Freed, A. M., & Bürgmann, R. (2004). Evidence of power-law flow in the Mojave Desert mantle. *Nature*, *430*(6999), 548–551. https://doi.org/10.1038/nature02784

Freed, A. M., Herring, T., & Bürgmann, R. (2010). Steady-state laboratory flow laws alone fail to explain postseismic observations. *Earth and Planetary Science Letters*, *300*(1–2), 1–10. https://doi.org/10.1016/j.epsl.2010.10.005

Freed, A. M., Hirth, G., & Behn, M. D. (2012). Using short-term postseismic displacements to infer the ambient deformation conditions of the upper mantle. *Journal of Geophysical Research*, *117*(B1), B01409. https://doi.org/10.1029/2011jb008562

Fukuda, J., & Johnson, K. M. (2021). Bayesian inversion for a stress-driven model of afterslip and viscoelastic relaxation: Method and application to postseismic deformation following the 2011 Mw 9.0 Tohoku-Oki earthquake. *Journal of Geophysical Research: Solid Earth*, *126*(5), e2020JB021620. https://doi.org/10.1029/2020JB021620

Fukuda, J., Muto, J., Koizumi, S., Sawa, S., & Nagahama, H. (2022). Enhancement of ductile deformation in polycrystalline anorthite due to the addition of water. *Journal of Structural Geology*, *156*, 104547. https://doi.org/10.1016/j.jsg.2022.104547

Fukuda, J.-I., Holyoke, C. W., III, & Kronenberg, A. K. (2018). Deformation of fine-grained quartz aggregates by mixed diffusion and dislocation creep. *Journal of Geophysical Research: Solid Earth*, *123*(6), 4676–4696. https://doi.org/10.1029/2017jb015133

Gleason, G. C., & Tullis, J. (1995). A flow law for dislocation creep of quartz aggregates determined with the molten salt cell. *Tectonophysics*, *247*(1–4), 1–23. https://doi.org/10.1016/0040-1951(95)00011-b

Griggs, D. (1967). Hydrolytic weakening of quartz and other silicates. *Geophysical Journal International*, *14*(1–4), 19–31. https://doi.org/10.1111/j.1365-246x.1967.tb06218.x

Griggs, D., & Blacic, J. (1965). Quartz: Anomalous weakness of synthetic crystals. *Science*, *147*(3655), 292–295. https://doi.org/10.1126/science.147.3655.292

Hansen, L. N., Kumamoto, K. M., Thom, C. A., Wallis, D., Durham, W. B., Goldsby, D. L., et al. (2019). Low-temperature plasticity in olivine: Grain size, strain hardening, and the strength of the lithosphere. *Journal of Geophysical Research: Solid Earth*, *124*(6), 5427–5449. https://doi.org/10.1029/2018jb016736

Hirth, G., & Kohlstedt, D. L. (2003). Rheology of the upper mantle and the mantle wedge: A view from the experimentalists. In J. Eiler (Ed.), *Inside the subduction factory* (Vol. 138, pp. 83–105). Am. Geophys. Soc.

Hirth, G., Teyssier, C., & Dunlap, J. W. (2001). An evaluation of quartzite flow laws based on comparisons between experimentally and naturally deformed rocks. *International Journal of Earth Sciences*, *90*(1), 77–87. https://doi.org/10.1007/s005310000152

Holyoke, C. W., III, & Kronenberg, A. K. (2010). Accurate differential stress measurement using the molten salt cell and solid salt assemblies in the Griggs apparatus with applications to strength, piezometers and rheology. *Tectonophysics*, *494*(1–2), 17–31. https://doi.org/10.1016/j.tecto.2010.08.001

Ji, S., Jiang, Z., Rybacki, E., Wirth, R., Prior, D., & Xia, B. (2004). Strain softening and microstructural evolution of anorthite aggregates and quartz–anorthite layered composites deformed in torsion. *Earth and Planetary Science Letters*, *222*(2), 377–390. https://doi.org/10.1016/j.epsl.2004.03.021

Ji, S., Mainprice, D., & Boudier, F. (1988). Sense of shear in high-temperature movement zones from the fabric asymmetry of plagioclase feldspars. *Journal of Structural Geology*, *10*(1), 73–81. https://doi.org/10.1016/0191-8141(88)90129-0

Jung, H., & Karato, S.-I. (2001). Water-induced fabric transitions in olivine. *Science*, *293*(5534), 1460–1463. https://doi.org/10.1126/science.1062235

Karato, S. (1998). *Micro-physics of post glacial rebound*. Trans. Tech. Publ.

Karato, S. (2008). *Deformation of earth materials: An introduction to the rheology of solid earth*. Cambridge University Press.

Karato, S. (2010). The influence of anisotropic diffusion on the high-temperature creep of a polycrystalline aggregate. *Physics of the Earth and Planetary Interiors*, *183*(3), 468–472. https://doi.org/10.1016/j.pepi.2010.09.001

Karato, S., & Jung, H. (2003). Effects of pressure on high temperature dislocation creep in olivine. *Philosophical Magazine*, *83*(3), 401–414. https://doi.org/10.1080/0141861021000025829

Karato, S.-I. (2021). A theory of inter-granular transient dislocation creep: Implications for the geophysical studies on mantle rheology. *Journal of Geophysical Research: Solid Earth*, *126*(10), e2021JB022763. https://doi.org/10.1029/2021jb022763

Kohlstedt, D. L. (2006). The role of water in high-temperature rock deformation. *Reviews in Mineralogy and Geochemistry*, *62*(1), 377–396. https://doi.org/10.2138/rmg.2006.62.16

Kronenberg, A. K., & Tullis, J. (1984). Flow strengths of quartz aggregates: Grain size and pressure effects due to hydrolytic weakening. *Journal of Geophysical Research*, *89*(B6), 4281–4297. https://doi.org/10.1029/jb089ib06p04281

Kruhl, J. H. (1987). Preferred lattice orientations of plagioclase from amphibolite and greenschist facies rocks near the insubric line (Western Alps). *Tectonophysics*, *135*(1–3), 233–242. https://doi.org/10.1016/0040-1951(87)90164-8

Linker, M. F., Kirby, S. H., Ord, A., & Christie, J. M. (1984). Effects of compression direction on the plasticity and rheology of hydrolytically weakened synthetic quartz crystals at atmospheric pressure. *Journal of Geophysical Research*, *89*(B6), 4241–4255. https://doi.org/10.1029/jb089ib06p04241

Luan, F., & Paterson, M. (1992). Preparation and deformation of synthetic aggregates of quartz. *Journal of Geophysical Research*, *97*(B1), 301–320. https://doi.org/10.1029/91jb01748

Masuti, S., & Barbot, S. (2021). MCMC inversion of the transient and steady-state creep flow law parameters of dunite under dry and wet conditions. *Earth Planets and Space*, *73*(1), 1–21. https://doi.org/10.1186/s40623-021-01543-9

Masuti, S., Barbot, S., Girard, J., & Karato, S. (2019). Anisotropic high-temperature creep in hydrous olivine single crystals and its geodynamic implications. *Physics of the Earth and Planetary Interiors*, *290*, 1–9. https://doi.org/10.1016/j.pepi.2019.03.002

Masuti, S., Barbot, S., Karato, S., Feng, L., & Banarjee, P. (2016). Upper-mantle water stratification inferred from observations of the 2012 Indian Ocean earthquake. *Nature*, *538*(7625), 373–377. https://doi.org/10.1038/nature19783

Masuti, S., Muto, J., & Rybacki, E. (2023a). Digitalized data for the transient creep of quartz and granulite at high temperature under wet conditions [Dataset]. Zenodo. https://doi.org/10.5281/zenodo.8304793

Masuti, S., Muto, J., & Rybacki, E. (2023b). Monte Carlo code for modelling the transient creep of different minerals [Software]. Zenodo. https://doi.org/10.5281/zenodo.8304760

Mehl, L., & Hirth, G. (2008). Plagioclase preferred orientation in layered mylonites: Evaluation of flow laws for the lower crust. *Journal of Geophysical Research*, *113*(B5), B05202. https://doi.org/10.1029/2007jb005075
Montardi, Y., & Mainprice, D. (1987). A transmission electron microscopic study of natural plastic deformation of calcic plagioclases (an 68-70). *Bulletin de Mineralogie*, *110*(1), 1–14. https://doi.org/10.3406/bulmi.1987.8022
Mulyukova, E., & Bercovici, D. (2022). On the co-evolution of dislocations and grains in deforming rocks. *Physics of the Earth and Planetary Interiors*, *328*, 106874. https://doi.org/10.1016/j.pepi.2022.106874
Muto, J., Hirth, G., Heilbronner, R., & Tullis, J. (2011). Plastic anisotropy and fabric evolution in sheared and recrystallized quartz single crystals. *Journal of Geophysical Research*, *116*(B2), B02206. https://doi.org/10.1029/2010jb007891
Muto, J., Moore, J., Barbot, S., Iinuma, T., Ohta, Y., & Iwamori, H. (2019). Coupled afterslip and transient mantle flow after the 2011 Tohoku earthquake. *Science Advances*, *5*(9), eaaw1164. https://doi.org/10.1126/sciadv.aaw1164
Okudaira, T., Takeshita, T., Hara, I., & Ando, J.-I. (1995). A new estimate of the conditions for transition from basal <a> to prism [c] slip in naturally deformed quartz. *Tectonophysics*, *250*(1–3), 31–46. https://doi.org/10.1016/0040-1951(95)00039-4
Olsen, T. S., & Kohlstedt, D. L. (1984). Analysis of dislocations in some naturally deformed plagioclase feldspars. *Physics and Chemistry of Minerals*, *11*(4), 153–160. https://doi.org/10.1007/bf00387845
Pabst, W., Gregorova, E., Rambaldi, E., & Bignozzi, M. C. (2015). Effective elastic constants of plagioclase feldspar aggregates in dependence of the anorthite content: A concise review. *Ceramics*, *59*, 326–330.
Passchier, C. W., & Trouw, R. A. (2005). *Microtectonics*. Springer Science & Business Media.
Poirier, J.-P. (1985). *Creep of crystals: High-temperature deformation processes in metals, ceramics and minerals*. Cambridge University Press.
Pollitz, F. F. (2003). Transient rheology of the uppermost mantle beneath the Mojave Desert, California. *Earth and Planetary Science Letters*, *215*(1–2), 89–104. https://doi.org/10.1016/s0012-821x(03)00432-1
Pollitz, F. F. (2005). Transient rheology of the upper mantle beneath central Alaska inferred from the crustal velocity field following the 2002 Denali earthquake. *Journal of Geophysical Research*, *110*(B8), B08407. https://doi.org/10.1029/2005jb003672
Pollitz, F. F., Kobayashi, T., Yarai, H., Shibazaki, B., & Matsumoto, T. (2017). Viscoelastic lower crust and mantle relaxation following the 14–16 April 2016 Kumamoto, Japan, earthquake sequence. *Geophysical Research Letters*, *44*(17), 8795–8803. https://doi.org/10.1002/2017gl074783
Qiu, Q., Moore, J. D., Barbot, S., Feng, L., & Hill, E. M. (2018). Transient rheology of the Sumatran mantle wedge revealed by a decade of great earthquakes. *Nature Communications*, *9*(1), 995. https://doi.org/10.1038/s41467-018-03298-6
Raterron, P., Amiguet, E., Chen, J., Li, L., & Cordier, P. (2009). Experimental deformation of olivine single crystals at mantle pressures and temperatures. *Physics of the Earth and Planetary Interiors*, *172*(1–2), 74–83. https://doi.org/10.1016/j.pepi.2008.07.026
Richter, B., Stünitz, H., & Heilbronner, R. (2018). The brittle-to-viscous transition in polycrystalline quartz: An experimental study. *Journal of Structural Geology*, *114*, 1–21. https://doi.org/10.1016/j.jsg.2018.06.005
Rutter, E., & Brodie, K. (2004). Experimental intracrystalline plastic flow in hot-pressed synthetic quartzite prepared from brazilian quartz crystals. *Journal of Structural Geology*, *26*(2), 259–270. https://doi.org/10.1016/s0191-8141(03)00096-8
Rybacki, E., & Dresen, G. (2000). Dislocation and diffusion creep of synthetic anorthite aggregates. *Journal of Geophysical Research*, *105*(B11), 26017–26036. https://doi.org/10.1029/2000jb900223
Rybacki, E., Gottschalk, M., Wirth, R., & Dresen, G. (2006). Influence of water fugacity and activation volume on the flow properties of fine-grained anorthite aggregates. *Journal of Geophysical Research*, *111*(B3), B03203. https://doi.org/10.1029/2005jb003663
Stünitz, H., Gerald, J. F., & Tullis, J. (2003). Dislocation generation, slip systems, and dynamic recrystallization in experimentally deformed plagioclase single crystals. *Tectonophysics*, *372*(3–4), 215–233. https://doi.org/10.1016/s0040-1951(03)00241-5
Tang, C.-H., Hsu, Y.-J., Barbot, S., Moore, J. D., & Chang, W.-L. (2019). Lower-crustal rheology and thermal gradient in the Taiwan orogenic belt illuminated by the 1999 Chi-Chi earthquake. *Science Advances*, *5*(2), eaav3287. https://doi.org/10.1126/sciadv.aav3287
Tokle, L., Hirth, G., & Behr, W. M. (2019). Flow laws and fabric transitions in wet quartzite. *Earth and Planetary Science Letters*, *505*, 152–161. https://doi.org/10.1016/j.epsl.2018.10.017
Trepmann, C., & Stöckhert, B. (2013). Short-wavelength undulatory extinction in quartz recording coseismic deformation in the middle crust–an experimental study. *Solid Earth*, *4*(2), 263–276. https://doi.org/10.5194/se-4-263-2013
Trepmann, C. A., Stöckhert, B., Dorner, D., Moghadam, R. H., Küster, M., & Röller, K. (2007). Simulating coseismic deformation of quartz in the middle crust and fabric evolution during postseismic stress relaxation-an experimental study. *Tectonophysics*, *442*(1–4), 83–104. https://doi.org/10.1016/j.tecto.2007.05.005
Tullis, J., Christie, J. M., & Griggs, D. T. (1973). Microstructures and preferred orientations of experimentally deformed quartzites. *Geological Society of America Bulletin*, *84*(1), 297–314. https://doi.org/10.1130/0016-7606(1973)84<297:mapooe>2.0.co;2
Tullis, J., Yund, R., & Farver, J. (1996). Deformation-enhanced fluid distribution in feldspar aggregates and implications for ductile shear zones. *Geology*, *24*(1), 63–66. https://doi.org/10.1130/0091-7613(1996)024<0063:defdif>2.3.co;2
Weertman, J. (1968). Dislocation climb theory of steady state creep. *Transactions of the American Society of Metals*, *61*, 681–694.
Yund, R. A., & Tullis, J. (1980). The effect of water, pressure, and strain on AL/SI order-disorder kinetics in feldspar. *Contributions to Mineralogy and Petrology*, *72*(3), 297–302. https://doi.org/10.1007/bf00376148
Závada, P., Schulmann, K., Konopásek, S., Ulrich, J., & Lexa, O. (2007). Extreme ductility of feldspar aggregates-Melt-enhanced grain boundary sliding and creep failure: Rheological implications for felsic lower crust. *Journal of Geophysical Research*, *112*(B10), B10210. https://doi.org/10.1029/2006JB004820
Zhou, Y., Zhang, H., Yao, W., Dang, J., & He, C. (2017). An experimental study on creep of partially molten granulite under high temperature and wet conditions. *Journal of Asian Earth Sciences*, *139*, 15–29. https://doi.org/10.1016/j.jseaes.2016.10.011